Inputs generation for COLISEUM coupling losses model using X-ray tomography: analytic and experimental approaches

R. Babouche, L. Zani, A. Louzguiti, B. Turck, J.L. Duchateau, F. Topin, I. Tiseanu, M. Lungu, D. Dumitru

Inputs generation for COLISEUM coupling losses model using X-ray tomography: analytic and experimental approaches

R. Babouche[1,2], L. Zani[1], A. Louzguiti[1], B. Turck[1], J.L. Duchateau[1], F. Topin[2], I. Tiseanu[3], M. Lungu[3], D. Dumitru[3]

[1]Commissariat à l'Energie Atomique et aux Energies Alternatives, Cadarache, 13108 St Paul-Lez-Durance, France
[2]Aix-Marseille Univ, CNRS, IUSTI, Marseille, France
[3]National Institute for Laser and Radiation Physics, INFLPR, 077125 Magurele, Romania

***Abstract*— Tokamaks coils are wound with long lengths of cables including hundreds of superconducting and copper strands twisted together into multiple stages. They refer to Cable In Conduit Conductors (CICC). Coupling losses induced by magnetic field variations dissipate power in the coils during machine operation. For several years, the CEA has been developing the analytical model COLISEUM (COupling Losses analytIcal Staged cablEs Unified Model) aiming at predicting coupling losses at various conductor scales. Geometrical (cabling radii, twist pitches) and electrical (inter-strand and inter-bundle conductances) parameters of each stage constitute the model inputs. In this article, we first present the raw 3D tomographic image treatment method that will serve to generate COLISEUM inputs with high level of reliability. We then define and extract several relevant effective geometric cable parameters from images data. These inputs are used along with the COLISEUM model to improve coupling losses prediction. A systematic study of six JT-60SA TF type samples has been realized and a geometric parameters database is constructed. The COLISEUM model is used in a 2-stage configuration with the two highest stages of the cable. First results are presented and discussed.**

***Index Terms*— Superconducting magnets, CICC, X-ray tomography, geometric parameters measurement, AC losses, modelling.**

I. Introduction

The COLISEUM (COupling Losses analytIcal Staged CablEs Unified Model) model [1]- [2] is a fully analytical model addressing the coupling losses for a complete Cable In conduit Conductor (CICC). The hysteretic losses are not considered in COLISEUM, which is based on currents loops flowing along hollow tubes of current. The last version addresses the coupling losses for a full CICC, accounting for contributions from the strand up to the n^{th}-stage of the cable. In this paper, we consider the coupling losses for a 2-stage configuration with the two highest stages of the cable. In a similar way as in MPAS [3]-[4], each stage is defined by two magnetic coefficients: a shielding coefficient, $n\kappa$ and a time constant, τ.

We present the method used to determine effective geometrical parameters (cabling radii and twist pitches) of the cable. Having access to tomographic 3D images of actual CICCs is an asset as the real strands trajectories can be fully recovered and used to compute losses. Those geometrical parameters allows us to remove the tangential constraint between stages previously used in COLISEUM [2].

II. Tomographic examinations of CICCs

A. Sample data base

In the framework of the collaboration between the CEA (France) and INFLPR (Romania), six JT-60SA TF type samples were examined using maximum 320 kV high penetration x-ray microtomograph [5]. For each sample, starting from 3D images, thousands of 2D slices (properly cleaned, normalized and cropped) are extracted. The scanned volume is 2000x2000xN voxels with N varying with the sample length. The voxel resolution is about ~20x20x110μm. The centre of each individual strand is identified on each slice, then individual strand trajectories are constructed. Centre radial displacement is about 3% to 6% of its diameter from one slice to another. The six samples named MAG42-1 to MAG42-6 [6] are made of 324 Nb-Ti superconducting strands and 162 copper strands of 0.81 mm diameter (cf. JT-60SA TF cable) see Table 1.

Table 1: Main characteristics parameters of the MAG42 samples [7].

Cable pattern	(2 Sc + 1 Cu)x3x3x3x6
Number of strands	486 (324 Sc + 162 Cu)
Twist pitches specifications [mm]	45-70-120-190-290

Sample lengths are about 300 mm corresponding to, at least, one last stage twist pitch. Therefore, they are representative of the real length conductor regarding losses measurements.

Table 2: MAG42 samples geometrical parameters

MAG42-	Ext. cross section (w/ jacket) [mm]	Corner radius (int/ext) [mm]	Void fraction [%]
#1	22.94 x 26.58	3.26 / 4.00	35.6
#2	22.28 x 26.52	2.29 / 3.56	33.2
#3	22.20 x 25.89	2.32 / 2.53	31.6
#4	22.04 x 25.70	1.99 / 2.20	30.2
#5	21.76 x 25.42	2.23 / 2.13	28.1
#6	21.30 x 25.37	2.23 / 2.02	25.9

Those samples present six different void fractions allowing us to study the effect on AC losses [6]. Table 2 presents, for each sample, their external cross-sections including the 2 mm thick stainless steel jacket, their void fraction and their corner radii. Those last one refer to the jacket radius at conductor corners and are manually determined from 2D slices. MAG42-3 sample

is representative of the produced JT-60SA TF coils conductors [7].

B. *Morphological analysis of the cables*

1) *Stage identification*

A group of three twisted strands refers to a triplet also called the first stage of the cable. This triplet is then twisted with two other triplets (triplet of triplets) also called second stage. This operation is repeated several times following the cable pattern presented in Table 1.

We present the post-treatment method applied to the six MAG42 samples. By means of the tomographic examinations, a large number of effective geometrical parameters can be determined. The outputs of the 2D slices coming from the tomographic examination are the coordinates of each strand centre at each slice. We have developed a tailored post-treatment process starting from these outputs. One of the main steps is to identify the different stages forming the cable. The method based on the mean distance between strands over the sample length is presented in [8]. To this day, the six MAG42 samples have been analysed and the five stages of each of them have been identified. Fig 1 shows tomographic 2D images of samples #1, #3 and #6. Similar tomographic images and stage identification overlays exist for the six MAG42 samples.

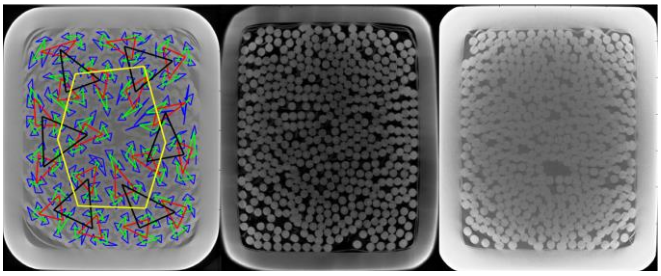

Fig 1: Left to right: MAG42 #1, #3, and #6. Sample #1 is displayed with the five identified stages using colour code: blue for the 1st stage (x3), green for the 2nd (3x3), red for the 3rd (3x3x3), black for the 4th (3x3x3x3) and yellow for the 5th (3x3x3x3x6). Pictures are chosen at random slice.

In Fig 1 left, each coloured polygon (connecting stage element centres) corresponds to one stage (see cable pattern in Table 1). The last one being a sextuplet, its figure is an hexagon. In each slice, barycentres are defined as the mean position of the strands belonging to a given stage. We have assessed those stages by checking that each triplet is made of two superconducting and one copper strands.

We have then determined one cabling radius and one twist pitch per stage. We define the cabling radius as the mean distance between the stage barycentre and the centre of strands forming that stage. The twist pitch is defined based on an external reference set on the cable axis and corresponds to one spatial period. One twist pitch is counted after one full rotation of the strands forming the stage around their barycentre. See Fig 2 a) where one 5th stage summit trajectory plotted against the sample length. In CICCs, strand or barycentre trajectories can be written as a sum of sine and cosine functions. The complex trajectory for a given element, k at a z location along the axis is [1]:

$$w_k(z) = x_k(z) + iy_k(z) \quad (1)$$

where,

$$x_k(z) = R_{c_k} cos\left(\frac{2\pi z}{l_{p_k}} + \varphi_k\right) \; ; \; y_k(z) = R_{c_k} sin\left(\frac{2\pi z}{l_{p_k}} + \varphi_k\right)$$

In equation (1), φ_k is the local phase shift and, R_{c_k} and l_{p_k} are respectively the cabling radius and the twist pitch of the considered element, k. To determine geometrical parameters of stages higher than the first one, barycentres are considered. In Fig 2a), one summit of the last stage of the cable is plotted along the cable axis. It refers to one barycentre of one fourth stage bundle. For each considered stage, strand or barycentre trajectory is represented by a perfect helicoid as shown in Fig 2a). A Fast Fourier Transform (FFT) algorithm is then applied to determine the parameters of interest. To obtain pure sinusoids, an iterative process starting from the highest stage is applied. We suppressed the component of the direct higher stage. Thus, results refer only to the component of the considered stage (see Fig 2b)). If we consider the third stage of the cable, there is 18 corresponding bundles, thus, 18 barycentres for which effective geometrical parameters are computed based on their trajectories. Each parameter follows a statistical distribution from which we took the mean value to determine one cabling radius and one twist pitch value. The associated standard deviations are also given. This method is applied for each stage and each sample.

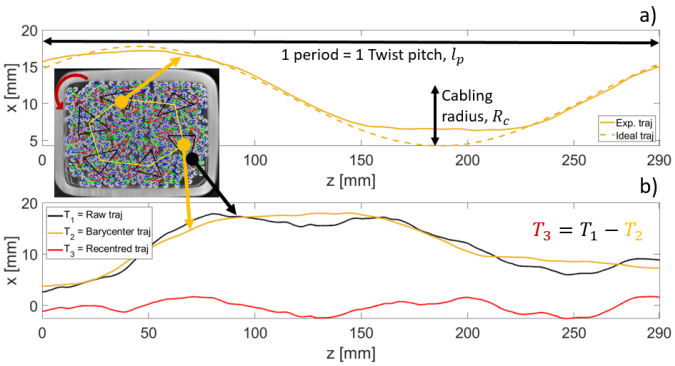

Fig 2: Example of MAG42-3 sample. (a) one last stage summit effective trajectory (solid line) and ideal helicoid trajectory (dashed line) along the sample length. (b) raw (black) and recentred (red) trajectories of the third stage barycenter using direct higher stage barycenter trajectory (yellow).

We have also developed a method based on geometrical analysis to determine both R_{c_k} and l_{p_k} where cabling radii and twist pitches are defined in the same way. In the following, we call these methods: "FFT" and "Geo". For a perfect helicoid, these methods were cross-checked and showed similar results. Nevertheless, some discrepancies may appear when considering the entire JT-60SA TF cable. It is due to the fact that the Fourier transform, considers only the maximum amplitude and spatial frequency of the maximum amplitude to extract respectively one cabling radius and one twist pitch. On the contrary, the second method considers the geometrical parameters at each slice of the sample and compute an average value. Thus, it takes into account each of their variations. In the following sections, cabling radii and twist pitches values computed with the both methods are presented. One should stressed out that we use these methods to determine "effective" parameters without a priori on the parameters values. Each

method have pros and cons and only losses computation will validate one or the other.

2) Cabling radii

The cabling radius, has an impact on coupling losses as it is directly linked to the shielding coefficient $n\kappa$ [1]. Below, cabling radii values among the six MAG42 samples coming from the FFT method (Table 3) and Geo method (Table 4) are presented.

Table 3: MAG42 samples cabling radii [mm] from FFT method

MAG42-	stg #1	stg #2	stg #3	stg #4	stg #5
#1	0.49±8%	0.76±5%	1.48±3%	2.57±3%	7.00
#2	0.51±6%	0.80±4%	1.54±2%	2.69±1%	7.22
#3	0.48±8%	0.76±4%	1.45±2%	2.50±2%	6.75
#4	0.48±8%	0.76±6%	1.47±3%	2.55±3%	6.83
#5	0.46±7%	0.74±6%	1.45±3%	2.49±3%	6.74
#6	0.48±7%	0.77±4%	1.46±3%	2.53±5%	6.71

Table 4: MAG42 samples cabling radii [mm] from Geo method

MAG42-	stg #1	stg #2	stg #3	stg #4	stg #5
#1	0.58±7%	1.00±3%	1.79±2%	3.09±1%	7.27
#2	0.59±6%	1.03±3%	1.84±3%	3.19±1%	7.46
#3	0.56±7%	0.98±3%	1.75±2%	3.00±1%	6.99
#4	0.57±7%	0.99±3%	1.77±3%	3.05±2%	7.07
#5	0.57±6%	0.99±3%	1.77±2%	3.03±2%	7.02
#6	0.58±6%	0.99±3%	1.77±3%	3.05±3%	7.04

Discrepancies between cabling radii values displayed in Table 3 and Table 4 are due to the computation method as explained in the previous section. MAG42 samples are composed of one last stage (last sextuplet, see Table 1), that is why no standard deviation is computed for the 5th stage. In Fig 2, the effective trajectory is approached by an ideal helicoid to determine its cabling radius. Nevertheless, it is worth pointing out, that between 150 and 250 mm, the apparent cabling radius is lower for the effective trajectory compared to the ideal one. This behaviour is linked to the rectangular shape of the conductor and mainly visible on the last stages cabling radii. Stages will tend to have a larger cabling radius along the sample long direction and lower one in the small direction leading to a more elliptical shape of the stages. To this day, we do not take into account such behaviour, nevertheless, this result will be used in future work to improve the COLISEUM model by adding inputs dependence with magnetic field variation direction.

In Table 3 and Table 4, it can be seen that the void fraction has apparently little effect on the values of the cabling radius of the four first stages, and only some effect on the very last stage. If we consider a triplet of strands (strand radius being equal to 0.405 mm) in tangent condition, the cabling radius would be equal to $R_c = r_{str}/\sin(\pi/3) = 0.47\,mm$. On the one hand, 1st-stages cabling radii are close to this value using the FFT method and, on the other hand, slightly larger using the Geo method. Overall, in those samples, 1st-stages are close to the tangent condition and do not much vary with the cable void fraction.

3) Twist pitches

The second geometrical parameter is the twist pitch. It has a direct impact on coupling losses through the time constant, τ [9] and [1]. In tables below, results among the six MAG42 samples are presented for each computation method.

Table 5: MAG42 samples twist pitches [mm] from the FFT method

MAG42-	stg #1	stg #2	stg #3	stg #4	stg #5
#1	44.4±3%	66.0±3%	122.7±6%	191.3±11%	280.5
#2	46.2±2%	68.6±3%	126.5±5%	211.9±6%	295.7
#3	43.9±3%	65.6±3%	122.8±5%	201.6±5%	284.1
#4	44.6±3%	66.4±4%	125.0±7%	213.9±10%	306.6
#5	44.5±3%	66.6±4%	126.6±7%	211.9±5%	296.8
#6	44.2±3%	64.8±4%	118.1±7%	189.4±5%	317.0

Table 6: MAG42 samples twist pitches [mm] from the FFT method

MAG42-	stg #1	stg #2	stg #3	stg #4	stg #5
#1	44.1±5%	61.4±6%	105.6±7%	169.5±7%	273.7
#2	45.5±4%	63.0±4%	107.6±4%	179.7±5%	294.0
#3	33.6±14%	47.9±9%	88.8±9%	151.1±9%	264.0
#4	43.5±5%	59.5±6%	104.2±6%	173.3±6%	295.5
#5	42.7±5%	59.0±5%	101.3±8%	166.8±5%	282.7
#6	43.1±6%	58.7±5%	99.1±5%	155.5±9%	300.2

From Table 5 and Table 6, it seems that the FFT based method gives results closer to manufacturer specifications (see Table 1) than the Geo method. The void fraction decreases from sample #1 to #6 (see Table 2). For the last stage, a clear trend of an increase of the effective twist pitch can be seen for both methods. This is in line with usual observations of an increase of last stage twist pitch after a compaction process. Note that, for the Geo based method (see Table 6), MAG42-3 sample shows lower values compare to the other samples. To this day, this behaviour is not clearly understood. The twist pitch computation allows to have information on the twisting direction: negative for the left-hand one and positive for the right-hand one. In our frame, we computed negative twist pitches and choose to present absolute values in the tables above. Those results are in line with manufacturer specifications [6].

4) Contact statistics

From the 486 strand trajectories we can compute the inter-strand contact width statistics (see schematic in Fig 3). The higher the contact width is, the more crushed the strands are. A similar study was conducted in [10] on samples #2 and #3. Fig 3 shows the number of contacts per slice for sample #1 to #6 as a function of the contact width. The strand diameter is noted d_{str} and d_0 is the distance between two strands centres. Strands centres are automatically identified by INFLPR using Hough transform algorithm. Nevertheless, for some strands, the centre identification is not nominal (i.e. centre shifted from the actual strand centre or the actual strand shape is slightly deformed) and may affect contact width computation. Therefore, we compute these statistics for a range of apparent diameter. We vary the diameter using a parameter, noted $\alpha \in [1; 1.1]$. Therefore, the strands contact width is computed as expressed in Fig 3.

The mean contact width values and associated standard deviation, for samples #1 to #6, are respectively 40.6±11.2%, 37.7±10.4%, 43.4±11.4%, 40.9±11.4%, 41.7±12.0% and 40.1±12.1%. The contact width is directly linked to the inter-strands resistance: the lower the contact surface is, the higher

the local resistance will be. We assume that sample void fraction would impact the contact statistics distribution in such a way that, the more compacted the sample is, the larger the mean contact width will be. Nevertheless, as presented in Fig 3, it seems that the contact width do not depend much on the sample void fraction.

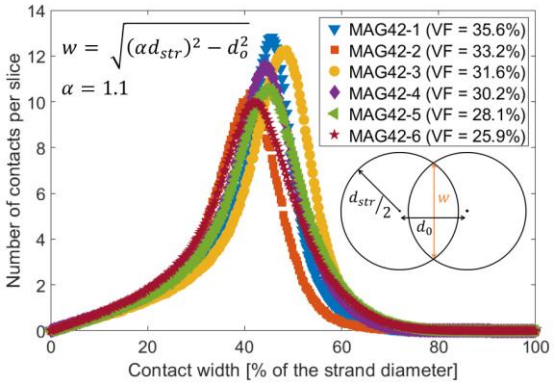

Fig 3: MAG42 samples contact width statistics (0.3% binning)

We assessed the impact of the α value on those results. In Fig 4, the left axis shows the mean contact width plotted against α values going from 1.0 to 1.1. The larger α is, the larger the contact area around each strand is, and therefore, the larger the mean contact width is. It is also interesting to look at the spread of these statistical distributions. It corresponds to the type of contacts that exist in the cable. A broader distribution would mean that a larger variety of contacts exist, thus, larger variety of inter-strands resistance. In Fig 4, the right axis shows the proportion of the standard deviation with regard to the mean value. That decreasing trend means that, the larger α is, the steeper are the distributions, which means that contacts variety become less important.

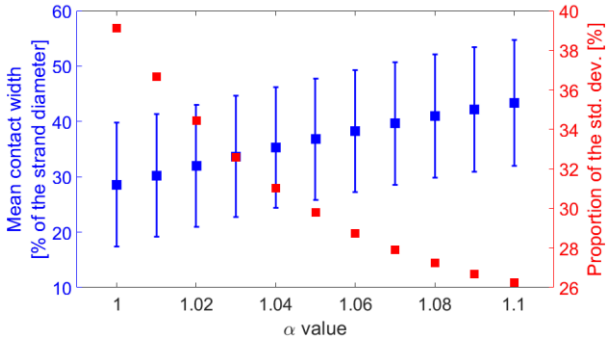

Fig 4: Left axis: mean contact width computed for α from 1.0 to 1.1. Right axis: proportion of the standard deviation with regard to the mean contact value. Computed on MAG42-3 sample.

In order to check that results presented in Fig 3 and Fig 4 are not biased by the strand type we discriminated the strands contact width as a function of the strand material (i.e. superconducting composite or copper strands). Results are shown in Fig 5. For each sample, copper strands are the most crushed ones (see black and blue symbols in Fig 5). In addition, the spread of those contacts are larger than for superconducting ones. We can explain this behaviour by the fact that the copper material is more ductile than the superconducting composite. On average over the six MAG42 samples, the penetration width between two superconducting strands is 3% lower than between a superconducting and a copper strand, and 4% lower than between two copper strands.

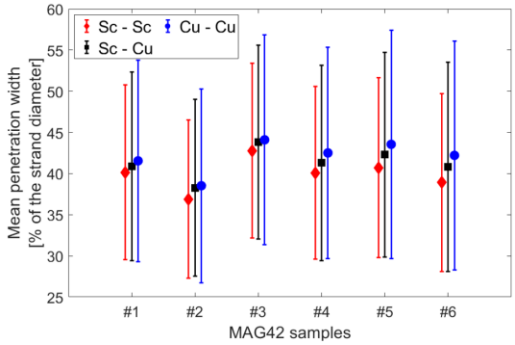

Fig 5: MAG42 samples mean penetration width as function of strand type.

To this day, we cannot conclude on the behaviour of the contact statistics as a function of the sample void fraction. The impact of the contact threshold might not be linear and therefore should be carefully considered. This topic will be further investigated. In the future, contact statistics will be used to build the equivalent electrical network of the cable. Strands will be selected based on their material type and stage identification to compute inter-strand resistances for several cases (within the same triplet, inter-stage etc.). These simulations will be reproduce in reality with a ~1m long JT-60SA TF type sample. Eventually, results will be compared and effective electrical parameters will be extracted to be used as COLISEUM model inputs.

5) Inter-strands distances statistics

The 486 strands forming the JT-60SA TF cable are twisted and gathered into stages resulting in complex trajectories. In this section we conduct a comparative study on the inter-strands distances among the six MAG42 samples. These distances are computed at each slice and gathered to be displayed in Fig 6. They are normalized to the strand diameter of 0.81 mm and plotted against the count at each distance value. Plotted lines are used to ease visualization and discriminate samples dynamics. The six distributions presented in Fig 6 have a strong asymmetric profile. Indeed, the lower the distances are, the more crushed against each other the strands are. This mechanical limit leads to a steep decrease toward low values. On the contrary, strands may be far from each other depending on the cable behaviour within the jacket, thus, leading to a less steep decrease toward high distances values. For these six distribution, the mean inter-strands distance values and associated standard deviations are displayed in the legend. In Fig 6, 100 % of the strand diameter (i.e. $d_{str} = d_o$ with d_{str} the strand diameter and d_0 the distance between two strands centres), corresponds to tangent strands. For illustration purpose, some inter-strands distances are plotted in the insert picture in Fig 6. Here, for each sample, the mean inter-strands distance value is around 120 % which is equal to 0.97 mm.

As in Fig 3, it is worth pointing out the unexpected behaviours of the samples MAG42-1, VF = 32.6% and MAG42-2, VF = 33.2%. While being more compacted, sample #2 shows a lower

contact width compared to sample #1 (see Fig 3), In addition, the mean inter-strands distance is larger in sample #2 (=129%) than in sample #1 (=125%). Similar unexpected observations exist while comparing samples #3 and #6.

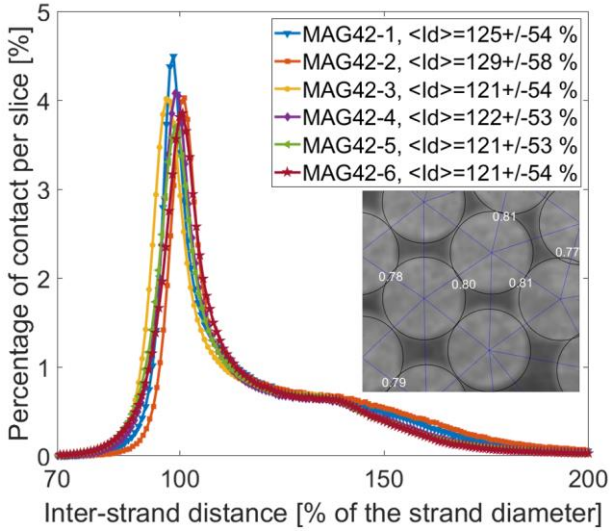

Fig 6: MAG42 samples inter-strands distances statistics (0.8% binning). Insert, some inter-strands distances expressed in mm for illustration.

The six MAG42 samples have been cut from the same cable length. From it, six equal lengths (about 1 meter long) have been cut, then separately inserted and compacted. The compaction rolls were adjusted to each sample in order to match with the target void fractions assigned to each of them. For each MAG42 sample, the definitive compaction was applied in one step through the rolling machine. Quality control was done on jacket external dimensions by the manufacturer. The output of that process is visible on the external sample shape as, for instance, sample #1 have more round corners compare to sample #6 with more sharp ones. One can look at the jacket corner radii values (see Table 2) to assess these observations. In future developments, we plan to investigate global and local voids of each MAG42 sample.

Considering that manufacturing process and surprising results on both contact width and inter-strands distance statistics, we conducted a preliminary investigation on global and local void fractions of MAG42-2 sample. First results seem to indicate that the manufacturing process have impacted the conductor jacket and reduced its width below the nominal 2 mm value. Therefore, although the MAG42-2 sample have an apparent lower external volume compare to MAG42-1 (see external dimensions measured in Table 2), the internal volume is not reduced and void fraction is higher from the expected one. A comprehensive study of void fractions and the impact of the manufacturing process on the conductor jacket will be conducted on each sample.

To conclude, conductor and cable dynamics under compaction are not easily predictable and these last observations may explain the unexpected statistics presented in Fig 3 and Fig 6.

III. Application to the COLISEUM model

A. *COLISEUM model in non-tangential conditions*

Real cables are compacted into stainless-steel jackets to form CICCs. The Fig 7 presents the JT-60SA TF cable in the frame of the COLISEUM model using tangent condition from the lowest stage, Fig 7a), and using cabling radii from tomographic data post-treatment (FFT method) for the MAG42-3 sample, Fig 7b).

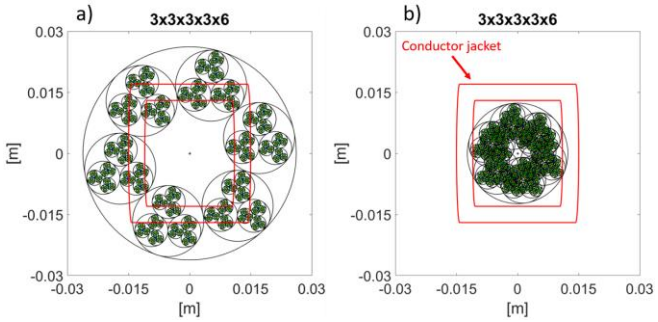

Fig 7: JT-6SA TF cable in the frame of the COLISEUM model: a) tangent condition; b) using cabling radii from tomographic data post treatment (for MAG42-3 sample FFT method, see Table 3).

Both configurations are compared with the conductor jacket displayed in red. In Fig 7a), the cable volume is larger than the jacket and the real cable leading to overestimate the losses. On the contrary, in Fig 7b), the cable volume is more realistic and should be more relevant regarding coupling losses. However, the use of effective geometrical parameters introduces some inter-penetration between elements. The COLISEUM model is therefore studied in this configuration to assess its use. Investigations have already been made on COLISEUM 2-stage in [8]. Because of the complexity of a five-stage cable geometry, we proceed here as a first step for the introduction of the tomographic parameters with a 2-stage configuration.

Here after, we consider a 2-stage cable made of a sextuplet of triplets (i.e. 3x6 configuration with N_1 = 3 and N_2 = 6). They correspond to the two highest stages of JT-60SA TF cable. Because they are contributing the most to the coupling losses, they are relevant of the real cable from that point of view. To introduce non-tangential conditions, we have defined penetration coefficients, noted $\gamma \in]0; 1]$, at each stage n.

$$R_{c_n} = \gamma_n R_{c_n\, tangent} \tag{2}$$

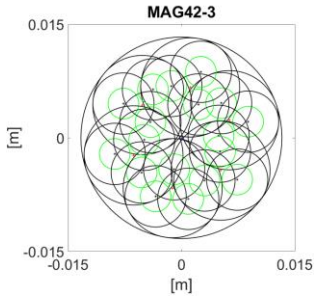

Fig 8: Two last stages of MAG42-3 sample represented in the COLISEUM model. Cabling radii are determined from tomographic data post-treatment using the FFT method, $R_{c_1} = 2.5\ mm, R_{c_2} = 6.75\ mm$ (see Table 3).

The lower γ is, the more penetrated the elements will be. In the following, γ_1 and γ_2 are respectively the first stage (triplet) and the second stage (sextuplet) penetration coefficients. It has been shown in [8] that, up to a certain penetration rate, even if the COLISEUM elements (strands or bundles of strands) penetrate each other the computation of the $(n\kappa, \tau)$ couples for each stage is not inconsistent. The Fig 8 shows the considered 2-stage cable.

By using cabling radii from the tomographic data post-treatment (Table 3 and Table 4), it is possible to compute the (γ_1, γ_2) couple using equation (2). Table 7 gathers γ_1 and γ_2 penetration coefficients coming from the Fast Fourier Transform based method and the geometrically based one.

Table 7: Penetration coefficient of the two last stages for both methods presented in II.B.1)

MAG42-	FFT method $\gamma_{1\,eq}$ / $\gamma_{2\,eq}$	Geo method $\gamma_{1\,eq}$ / $\gamma_{2\,eq}$
#1	0.55 / 0.40	0.66 / 0.42
#2	0.57 / 0.41	0.68 / 0.43
#3	0.53 / 0.39	0.64 / 0.40
#4	0.54 / 0.39	0.65 / 0.41
#5	0.53 / 0.39	0.65 / 0.40
#6	0.54 / 0.38	0.65 / 0.40

As shown in equation (2), penetration coefficients linearly depend on cabling radii determined by each method. It leads to some discrepancies on the (γ_1, γ_2) couples. For a specific method, because cabling radii are not much varying between samples (see Table 3 and Table 4), penetration coefficients are all in the same range and close from one sample to another. As in section II.B.2), there is no clear trend on the effect of the cable compaction on those coefficients.

B. Tomographic data as model inputs

In this section we present how effective geometrical parameters from tomographic data post-treatment are used as model inputs to compute coupling losses. We consider that COLISEUM model outputs are consistent if there is no negative or null $n\kappa$ and/or τ coefficients. We assume that using effective parameters inputs would bring coupling losses predictions close to experimental results. Before tomographic examinations of CICCs, twist pitches were taken from manufacturer specifications and cabling radii were determined assuming tangent elements from the lowest cable stage. Electrical input parameters correspond the inter-stages conductances, noted σ_1 and σ_2. They are set equal to $3 \times 10^8\ S/m$ for both stage and for any (γ_1, γ_2) combination. In this paper, the cable is compacted due to the effective geometrical parameters, thus, we adapted the inter-stage conductances to obtain magnetic coefficients values $(\sum n\kappa_i\tau_i)$ in line with data from bibliography [4].

In the following, we compute with the COLISEUM model the $(n\kappa, \tau)$ couples of each sample for both tomographic data analysis methods. The set of input parameters refers to: the stage multiplicity N, the cabling radii R_c, the twist pitches l_p and the inter-stage conductance σ, each of them taken for each stage. For the FFT method, cabling radii and twist pitches are taken from Table 3 and Table 5. For the Geo method, effective parameters are taken from Table 4 and Table 6. Those magnetic coefficients are gathered in Table 8 with, $n\kappa$ coefficients given per unit volume of cable.

Table 8: Computed magnetic coefficients for each tomographic analysis methods expressed per unit volume of cable

MAG42	FFT method		Geo method	
	τ_1 / τ_2 [ms]	$n\kappa_1$ / $n\kappa_2$	τ_1 / τ_2 [ms]	$n\kappa_1$ / $n\kappa_2$
#1	98 / 331	1.6e-5 / 1.03	61 / 297	0.010 / 0.98
#2	113 / 383	0.002 / 1.03	69 / 341	0.011 / 0.98
#3	103 / 349	0.001 / 1.02	50 / 263	0.020 / 0.97
#4	117 / 403	0.0004 / 1.02	64 / 335	0.017 / 0.97
#5	113 / 383	0.001 / 1.02	59 / 308	0.017 / 0.97
#6	100 / 389	0.008 / 1.01	55 / 323	0.035 / 0.95

The shielding coefficient, $n\kappa$ translates the ability of one stage to shield itself from an external magnetic field variation. For a dipole, the shielding is perfect and equal to 2. In Table 8, $n\kappa_2$ values are larger than $n\kappa_1$ ones, thus, one can say that the second stage of the cable is contributing the most the generated losses. Due to their similar geometrical characteristics and same electrical parameters, magnetic coefficients are close to each other among the six MAG42 samples. Considering the tangent cable, $n\kappa_1$ and $n\kappa_2$values are respectively equal to 0.0012 and 1.22 while time constants are equal to τ_1 = 158 ms and τ_2 = 357 ms. From Table 8, we can assess that the COLISEUM model does not show inconsistent magnetic coefficients when effective parameters are used as model inputs.

Table 9: $n\tau$ values ($= \sum n\kappa_i\tau_i$) for each tomographic analysis methods expressed per unit volume of cable

MAG42-	$n\tau$ [ms]	
	FFT method	Geo method
#1	341	293
#2	394	336
#3	357	256
#4	413	326
#5	393	299
#6	394	309

In Table 9, we computed the $\sum n\kappa_i\tau_i$ sum which is equivalent to the commonly used $n\tau$. Considering the tangent case, $n\tau$ value is equal to 436 ms. These values rely on the chosen inter-stage conductance, thus, they are shown only to provide an example of the COLISEUM model output. We plan in the future to measure effective inter-strand and inter-stage conductance to use them as electrical input parameters for the COLISEUM model.

C. Coupling losses computation using COLISEUM model

Using the magnetic coefficients computed in Table 8 we compute the associated coupling losses of that two stages cable. Results are compared between the tangent COLISEUM model and the compacted model using effective geometrical parameters as inputs taken from the two methods presented in II.B.1). A first comparison on the first two stages of the JT-

60SA TF cable was conducted in [8] using arbitrary penetration coefficients to simulate a compacted cable.
Coupling losses expressed per unit volume of cable are the sum of the losses at each stage and are given by

$$Q_{total\ cable} = \sum_{j=1}^{j=2} n\kappa_j \tau_j \frac{B_m^2}{\mu_0} \frac{\pi\omega}{1+(\omega\tau_j)^2} \quad (3)$$

where, $(n\kappa_j,\tau_j)$ couples are the magnetic coefficients of the j[th] stage and B_m is the amplitude of the external sinusoidal varying magnetic field. In addition, using equation (3), coupling losses expressed per unit volume of superconducting strands are given by

$$Q_{total\ Sc\ str} = Q_{total\ cable} \times r \quad (4)$$

with,

$$r = \frac{V_{cable}}{V_{Sc\ str}} = \frac{\pi L(R_{elem}+R_{c1}+R_{c2})^2}{\pi L N_{Sc\ str} r_{str}^2}$$

With, $N_{Sc\ str}$ the number of superconducting strands in the JT-60SA TF cable equal to 324 (see Table 1), r_{str} their radius and R_{elem} corresponds to the radius of the elements forming the first stage triplets (see insert schematic in Fig 9). In this application it is computed as the sum of the sub-stages cabling radii such as

$$R_{elem} = r_{str} + \sum_{j=1}^{3} R_{cj} \quad (5)$$

In the COLISEUM model, current loops are flowing through hollow tubes displayed in green in Fig 7, 8 and 9. Their radius is noted R_f. As a first approach, one can estimate that these current will flow at the direct sub-stage mean radius. Therefore, R_f radius will be taken equal to R_{c3} in this application. These two way of determining R_{elem} and R_f are based on geometrical assumptions as first developed in [1]. Another method, based on magnetic considerations can be considered and developed in [2]. For the tangent, FFT and Geo methods, cable volumes are respectively equal to 2165 mm^3, 479 mm^3 and 588 mm^3. Cabling and elements radii as well as the other inputs parameters to compute coupling losses with the COLISEUM model are gathered in Table 10.

Table 10: Considered parameters to compute coupling losses with the COLISEUM model.

Parameter	Tangent	FFT	Geo
N_1/ N_2	3 / 6	3 / 6	3 / 6
γ_1 / γ_2	1 / 1	0.53 / 0.39	0.64 / 0.40
R_{elem} [mm]	4.05	3.10	3.69
R_f [mm]	2.17	1.45	1.75
R_{c1} / R_{c2} [mm]	4.70 / 17.50	2.50 / 6.75	3.00 / 6.99
r	12.97	2.87	3.52
l_{p1} / l_{p2} [mm]	190 / 290	201.6 / 284.1	151.1 / 264.0
$\sigma_1 = \sigma_2$ [S/m]	3×10^8	3×10^8	3×10^8
$n\kappa_1$ / $n\kappa_2$	0.0012 / 1.22	0.0008 / 1.02	0.0205 / 0.97
τ_1 / τ_2 [ms]	158 / 357	103 / 349	50 / 263

Inter-stages conductances are similar to the ones used in the previous section, i.e. $\sigma_1 = \sigma_2 = 3 \times 10^8$ S/m and equal for the tangent and compacted cases.

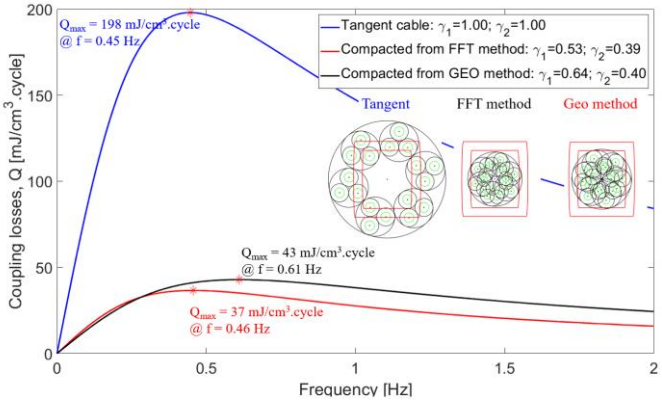

Fig 9: Total coupling losses computed for the tangent and compacted cases of MAG42-3 sample as a function of the frequency of the external magnetic field. Results expressed per unit volume of superconducting strands for a sinusoidal field amplitude of $B_m = \pm 0.1\ T$.

Fig 9 shows the computed coupling losses using the COLISEUM model for each cable considering input parameters from the MAG42-3 sample. These losses are expressed per unit volume of superconducting strands using equation (4). Note that, in Fig 9, only the total losses are displayed without the contributions of each stage. The coupling losses associated to the tangent cable, reach a maximum value of 198 mJ/cm^3.cycle at a frequency of 0.45 Hz. These losses decrease to 37 mJ/cm^3.cycle at a frequency of 0.46 Hz for the compacted cable using penetration coefficients from the FFT based method. On the other hand, for the compacted cable using the geometrically based method, maximum losses are equal to 43 mJ/cm^3.cycle at a frequency of 0.61 Hz.
The tangent model leads to a larger cable size compare the compacted ones. Thus, a larger magnetic flux is enclosed and, all things being equal, higher coupling losses are computed. From this point of view, the COLISEUM model is therefore consistent when using effective geometrical parameters as inputs. Maximum coupling losses computed for the tangent cable are 5.3 times higher than the ones computed from the FFT method. Regarding the volumes ratio, tangent cable is 4.5 larger than the compacted cable. Therefore, the ratio of the maximum coupling losses is in a 15% agreement range with the ratio of the cable volumes. Similar agreement (~20%) in found with the cable compacted using the geometric method.
In the future, COLISEUM model using effective geometrical parameters as inputs will be applied on a full JT-60SA TF cable and compared with AC losses measurements. The most relevant method to determine input parameters will be selected. In addition, inter-stage conductances will be measured and used as effective electrical input parameters.

IV. Conclusion and Perspectives

We have developed a dedicated post-treatment algorithm to study tomographic examination of CICCs. We have built a data

base gathering indicators and cable characteristics of six JT-60SA TF type samples. These data could be used as production monitoring indicators for manufacturers. The five stages forming MAG42 samples were identified and validated. For each of them, effective geometrical parameters were computed from two different methods and used as geometrical inputs in the COLISEUM model. We have also shown that the use of the model with non-tangential condition does not show any inconsistent magnetic coefficients values. Furthermore, we computed coupling losses for tangent and compacted cables as test cases and notice the consistent decrease of the losses due to the smaller cable size. In the future, the use of effective geometrical parameters will be extended to the full cable scale and comparison between COLISEUM model and AC losses measurements of MAG42 samples will be conducted.

Eventually, the study of the tomographic data, especially the contact statistics, will be applied to a ~1m long JT-60SA TF sample and used to determine an equivalent electrical network of the cable. This work will be associated with inter-strands resistances measurements to determine effective electrical inputs parameters for the COLISEUM model. Finally, the post-treatment algorithm for tomographic data will be applied to larger and more complex cables.

ACKNOWLEGMENT

Authors thank Slim Constants from ASSYSTEM for the financial and technical support. This work has been carried out within the framework of the EUROfusion Consortium, funded by the European Union via the Euratom Research and Training Programme (Grant Agreement No 101052200 — EUROfusion). Views and opinions expressed are however those of the author(s) only and do not necessarily reflect those of the European Union or the European Commission. Neither the European Union nor the European Commission can be held responsible for them.

REFERENCES

[1] A. Louzguiti, “Magnetic screening currents and coupling losses induced in superconducting magnets for thermonuclear fusion,” *PhD Thesis,* 2017.

[2] M. Chiletti, “Coupling losses in large superconducting Cable In Conduit Conductors for fusion reactors: analytical modelling and experimental investigations,” *PhD Thesis,* 2020.

[3] B. Turck and L. Zani, “A macroscopic model for coupling current losses in cables made of multi-stages of superconducting strands and its experimental validation,” *IEEE Transactions on Applied superconductivity,* vol. 18, no. 1, pp. 18-28, 2008.

[4] J. Duchateau, B. Turck, A. Torre and L. Zani, “An analytical model for coupling losses in large conductors for magnetic fusion,” *Cryogenics,,* vol. 120, 2021.

[5] I. Tiseanu, “Multi-scale 3D modelling of a DEMO prototype cable from strand to full-size conductor based on X-ray tomography and image analysis,” *Fusion Engineering and Design,* vol. 146, pp. 568-573, 2019.

[6] M. Chiletti, L. Zani, B. Turck, J. Duchateau and F. Topin, “Void Fraction Influence on CICCs Coupling losses: Analysis of Experimental Results With MPAS Model,” *IEEE Transactions on Applied Superconductivity,* vol. 30, no. 4, pp. 1-5, 2020.

[7] L. Zani, P. Barabaschi and M. Peyrot, “Starting EU Production of Strand and Conductor,” *IEEE Transaction on Applied Superconductivity,* vol. 22, no. 3, 2012.

[8] R. Babouche, L. Zani, A. Louzguiti, B. Turck, J. Duchateau and F. Topin, “Analytical Modeling of Coupling Losses in CICCs, Extensive Study of the COLISEUM Model,” *IEEE Transactions on Applied Superconductivity,* vol. 32, no. 6, pp. 1-5, 2022.

[9] M. Wilson, Superconducting Magnets, New York: Oxford University Press Inc., 1983.

[10] L. Zani, M. Chiletti, D. Dumitru, M. Lungu, I. Tiseanu and F. Topin, “Extensive analyses of superconducting cables 3D geometry with advanced tomographic examinations,” *IEEE Transactions on Applied Superconductivity,* vol. 31, no. 5, pp. 1-5, 2021.